

$TNF^{\Delta ARE}$ Pigs: A Translational Crohn's Disease Model

Thomas Winogrodzki^{a,*}, Amira Metwaly^{b,*}, Alessandro Grodziecki^a, Wei Liang^a,
Bernhard Klinger^a, Tatiana Flisikowska^a, Konrad Fischer^a, Krzysztof Flisikowski^a, Katja Steiger^c,
Dirk Haller^{b,*}, Angelika Schnieke^{a,*}

^aChair of Livestock Biotechnology, School of Life Sciences, Technical University of Munich, Freising, Germany

^bChair of Nutrition and Immunology, School of Life Sciences, Technical University of Munich, Freising, Germany

^cComparative Experimental Pathology, Institute of Pathology, Technical University of Munich, Munich, Germany

Corresponding author: Prof. Angelika Schnieke, Chair of Livestock Biotechnology, TU München, Liesel-Beckmann-Strasse 1, 85354, Freising, Germany. Tel: +49 8161 712004; Fax: +49 8161 712108; Email: a.schnieke@tum.de.

*These authors contributed equally to this work.

Abstract

Background and Aims: Crohn's disease [CD] is a major subtype of inflammatory bowel diseases [IBD] with increasing incidence and prevalence. Results of studies using available small and large animal models are often poorly translatable to patients, and few CD models show small intestinal pathology. Due to its similarities to humans, the pig has emerged as a highly suitable translational disease model, particularly for testing novel nutritional and technological interventions. Our goal was to develop a physiologically relevant porcine CD model to facilitate translation of findings and interventions towards the clinic.

Methods: We generated pigs bearing a 93-bp deletion of the adenosine–uracil-rich element [ARE] and a constitutive-decay element within the 3' untranslated region of the *TNF* gene. Comparative analysis of physiological, molecular, histological and microbial characteristics was performed between wild-type, $TNF^{\Delta ARE/+}$ and $TNF^{\Delta ARE/\Delta ARE}$ animals. Alterations in the microbiome were compared to the $TNF^{\Delta ARE}$ mouse model and IBD patients.

Results: $TNF^{\Delta ARE}$ pigs recapitulate major characteristics of human CD, including ulcerative transmural ileocolitis, increased abundance of proinflammatory cytokines, immune cell infiltration and dysbiotic microbial communities. 16S rRNA gene amplicon sequencing revealed enrichment in members belonging to *Megasphaera*, *Campylobacter*, *Desulfovibrio*, *Alistipes* and *Lachnospirillum* in faecal or mucosa-associated bacteria compared to wild-type littermates. Principal components analysis clustering with a subset of $TNF^{\Delta ARE/+}$ mice and human IBD patients suggests microbial similarity based on disease severity.

Conclusions: We demonstrate that the $TNF^{\Delta ARE}$ pig resembles a CD-like ileocolitis pathophenotype recapitulating human disease. The ability to conduct long-term studies and test novel surgical procedures and dietary interventions in a physiologically relevant model will benefit future translational IBD research studies.

Key Words: Inflammatory bowel disease [IBD]; Crohn's disease; pig/swine model

1. Introduction

Crohn's disease [CD] is one of the two main subtypes of inflammatory bowel diseases [IBD] characterized by patchy transmural inflammation in the entire digestive tract, predominantly affecting the terminal ileum and proximal colon.¹ CD is a multifactorial disease driven by complex gene–environment interactions following patterns of industrialization.² Genome-wide association studies have identified a variety of genetic risk alleles pointing towards a disruption of microbe–host interactions.³ The underlying molecular mechanisms of IBD and specific microbial and metabolic signatures have been elucidated using spontaneous, chemically induced and genetically engineered mouse or large animal models.^{4–6} However, CD-like inflammation with manifestation of small intestinal disease rarely occurs in currently available animal models of IBD, with mouse models being the most widely applied [e.g. SAMP/YitFc, *Xiap*^{-/-}, *Xbp1*^{-/-}, $TNF^{\Delta ARE}$]. Yet, due to their short lifespan and size, mouse models are of limited use

for the assessment of human-scale technologies and methods and in some cases are less suitable as disease models compared to species that are genetically, physiologically and anatomically more closely related to humans.^{7,8}

Our goal was therefore to generate a physiologically relevant animal model that reflects the human disease phenotype of CD as accurately as possible. It should be able to predict the influence of altered nutrition or microbiome on human or animal health and should represent a reliable preclinical model to assess new therapeutic approaches. Because of their comparatively large size and lifespan, large animal models are particularly well suited for testing technologies and methods developed for human clinical use, as well as for long-term studies and the collection of multiple fluid or tissue biopsies from a single animal, consistent with the 3Rs rules—replacement, reduction, refinement.⁹ In the past, in particular non-human primates [NHPs] and dogs have been used as large animal models for preclinical research because

they spontaneously develop IBD.^{5,6} However, animal studies with NHPs, despite their obvious similarities to humans, are ethically controversial, costly and carry the risk of transmitting zoonotic diseases.¹⁰ Canines are highly sensitive to intestinal disease and, therefore, often suffer from high mortality rates, mainly due to intestinal ischaemia. This is in addition to society's growing rejection of animal testing on dogs.¹⁰ On the other hand, the pig has emerged as an exceptionally well-suited large animal model for intestinal diseases because of its strong physiological, anatomical, genomic, immunological and nutritional similarities to humans. Porcine models have long been used to study the effect of human nutrition on metabolic syndromes, obesity and food allergies.¹¹ Both pig¹² and human bacterial libraries¹³ are available to elucidate the effect of specific bacterial strains on IBD. Pigs can be fed a human diet and faecal microbiota transfer from humans to pigs results in a gut microbiota closely resembling that of the human donor.^{14,15} A recent study of a large pig population assessed the effect of host genotype on the composition of the intestinal microbiota, demonstrating the high value and applicability of digestive disease research.¹⁶ Being also used for food production the opposition towards porcine models, especially in areas of great clinical need, is considerably lower compared to dogs or NHPs.

Here we report the generation and characterization of a porcine model for CD carrying a 93-bp deletion in the 3'-untranslated region [UTR] of *TNF* [*TNF α*], which deleted the transcript-stabilizing AU-rich element [ARE] and a constitutive decay element [CDE] similar to the *TNF^{FARE}* mouse model.

2. Materials and Methods

2.1. Ethics statement

Animal experiments were approved by the Committee on Animal Health and Care of the local government body of the state of Upper Bavaria [ROB 55.2-2532.Vet_02-18-56, 55.2-1-54- 2531-99-13] and performed according to the German Animal Welfare Act and European Union Normative for Care and Use of Experimental Animals.

2.2. Generation of *TNF^{FARE}* pigs

For CRISPR/Cas9-mediated excision of the 93-bp fragment containing the ARE and CDE1 element, two single guide RNAs [sgRNAs] were designed using CRISPOR.¹⁷ Both U6-gRNA-scaffold sequences were cloned into px330-U6-Chimeric_BB-CBh-hSpCas9 plasmid2 [Addgene no. 42230] [pX330-2gRNAs]. The px330-2gRNAs plasmid DNA was microinjected into *in vitro* fertilized porcine oocytes followed by laparoscopic embryo transfer, as previously described.^{18,19} Genomic DNA was isolated from ear biopsies using a GenElute Mammalian Genomic DNA Kit [Sigma]. Detection of the 93-bp deletion was determined by PCR using GoTaq polymerase [Promega] and primer pairs: Fwd: 5'-GGGTTTGGATTCTGGATGC-3', Rev: 5'-GCGGTTACAGACACAAC-3'. Thermal cycling parameters were: 95°C, 2 min; [35 \times] 95°C, 45 s, 60°C, 45 s, 72°C, 30 s; 72°C, 5 min. Amplicons were verified by Sanger sequencing [Eurofins Genomics]. sgRNA off-target sites were predicted using CRISPOR. Five highest scoring potential off-targets were analysed by PCR and Sanger sequencing.

2.3. Macrophage culture and RNA half-life analysis

EDTA-blood was collected from anaesthetized pigs. Peripheral blood mononuclear cells [PBMCs] were isolated by Ficoll-density gradient centrifugation. PBMCs were cultured in 10 mL RPMI 1640, 10% fetal calf serum [FCS], 1% GlutaMax [Sigma], 1% Pen-Strep/Amphotericin B and 10⁴ U/mL recombinant poGM-CSF [Biotechne] for 7 days. Macrophages were divided into four groups: [1] no supplements, [2] supplemented with 0.1 μ g/mL lipopolysaccharide [LPS; InvivoGen], [3] with LPS and 150 μ g/mL Polymyxin B [Invivogen] and [4] with LPS and after 45 min with 10 μ g/mL Actinomycin D [Calbiochem]. Macrophages were harvested at 0, 45 and 90 min and frozen at -80°C until processing.

2.4. RNA isolation and quantification

RNA was isolated from gut mucosal biopsies using a Monarch Total RNA Miniprep Kit [NEB] according to the manufacturer's protocols. cDNA was generated using LunaScript RT Master Mix Kit [NEB] according to the manufacturer's protocol. Real-time quantitative PCR [qPCR] was performed using the Fast SYBR Green Master Mix [Sigma] in a QuantStudio 5 Real-Time-PCR-Cycler [ThermoFisher Scientific] and the following primer pairs: *TNF*, Fwd: 5'-GGGCTTATCTGAGGTTTGGAG-3', Rev: 5'-TTCTGCCTACTGCACTTCGA-3'; *IL6*, Fwd: 5'-TCTGCAATGAGAAAGGAGATGTG-3', Rev: 5'-AGGTTCAAGTTGTTTTCTGCC-3'; *IL8*, Fwd: 5'-CTGTGAGGCTGCAGTTCTG-3', Rev: 5'-GTGATTGAGAGTGGACCCCA-3'. For transcript normalization, housekeeping genes GAPDH [Fwd: 5'-TTCCACGGCACAGTCAAGGC-3', Rev: 5'-GCGGTTACAGACACAAC-3'], β -actin [Fwd: 5'-TCCCTGGAGAAGAGCTACGA-3', Rev: 5'-GCAGGTCAGGTCCACAAC-3'] and RPS28 [Fwd: 5'-GTTACCAAGTTCTGGGCAG-3', Rev: 5'-CAGATATCCAGGACCCAGCC-3'] were selected based on NormFinder and BestKeeper.^{20,21} One-way ANOVA was performed, followed by Tukey's test for statistical evaluation using GraphPad Prism 8.

2.5. Protein quantification via Western blot

Ileal and colonic proteins were obtained by tissue homogenization in NP-40 buffer with 1 \times cComplete Mini Protease Inhibitor Cocktail [Roche]. Protein concentrations were determined using the Bradford assay. Protein lysates were separated by semi-dry Western blot (anti-TNF, 1:1000, Invitrogen [14-7321-85]; anti-GAPDH, 1:3000, Sigma [G8795]; anti-ZO1, 1:250, ThermoScientific [61-7300]; anti-occludin, 1:666, LSBio [LS-B5737]). Blots were developed using Pierce ECL Plus Western Blotting Substrate [ThermoScientific].

2.6. Protein quantification via ELISA

Faecal calprotectin content was measured by using faecal water and a pig calprotectin ELISA Kit [Cusabio, CSB-EQ013485PI]. Faecal water was isolated by diluting 50 mg of faeces in 400 μ L PBS followed by thorough vortexing. Homogenates were centrifuged at 500 g for 5 min, and the supernatant was collected for a second round of centrifugation at 6000 g for 5 min. The supernatant was 5-fold diluted in 1 \times assay reagent for protein quantification.

2.7. Histology and immunohistochemistry

Macroscopic findings during necropsy were documented, and images were reviewed by a board-certified veterinary pathologist. Representative specimens for histology were collected from rectum, proximal colon, caecum, distal ileum, proximal jejunum and proximal duodenum, fixed in 10% neutral-buffered formalin and embedded in paraffin [FFPE]. H&E-stained tissue sections [2 µm] were assessed for histological changes. Immunohistochemical stainings were performed on 3.5-µm FFPE tissue sections as described previously²² using the following antibodies: anti-Ki67, 1:300, Invitrogen [MA5-14520]; anti-CD3, 1:100, Southern Biotech [4511-01]; and anti-IBA1, 1:2000, Wako FujiFilm [019-19741]. Periodic Acid-Schiff-Alcian blue [Pas/AB] staining was performed as previously described.²² Quantification of lamina propria CD3 [T-cells] and IBA1 [macrophages] was performed on randomly selected areas and the ratio of positive/negative cells was calculated. Pas/AB⁺ and crypt Ki67⁺ cells were quantified by counting positive cells per crypt area. Statistical evaluation was performed as described above. Immunofluorescence staining was performed on 3.5-µm FFPE colonic sections using the following antibodies: anti-ZO1, 1:50, ThermoScientific [61-7300]; anti-occludin, 1:100, LSBio [LS-B5737]; and goat-anti-rabbit-Alexa Fluor Plus 594, 1:100, Invitrogen [A11012]. Confocal laser scanning microscopy was performed with an Olympus FV 3000 confocal microscope with a 60×/NA1.2/WD0.28 UPLSAPO60XS2 objective and water immersion lens, Olympus four-channel TruSpectral detection system and the Olympus FV 3000 Imaging Software, Cells Desktop Version 1 of the Center for Advanced Light Microscopy [CALM, Technical University of Munich, Germany].

2.8. Porcine samples for microbiota profiling

Wild-type and *TNF^{ΔARE}* littermate pigs were co-housed at the Technical University of Munich. No anti-diarrhoeal medication was administered. Piglets were raised with their mothers until weaning. All pigs received vaccinations against *Lawsonia intracellularis*, pneumococcal disease [pneumococcal polysaccharide vaccine, PPV], porcine reproductive and respiratory syndrome [PRRS], influenza, mycoplasma and porcine circovirus type 2 [PCV2]. All animals received the same diet [HEMO U 134 pellets; LikaWest] and water *ad libitum*. Faeces were collected and consistency was assessed monthly starting shortly after birth by digital sampling. Gut luminal and mucosal tissue samples were collected together with control samples of ambient air during necropsy and stored in Lysing Matrix B tubes [MP Biomedicals] filled with 500 µL Stool DNA Stabilizer [Invitex] at -80°C for downstream analysis.

2.9. Murine samples for microbiota profiling

TNF^{ΔARE} mice and wild-type littermates were imported from Case Western Reserve University, Cleveland, and housed under germ-free [GF] conditions. To establish a specific-pathogen-free [SPF] microbiota-colonized colony, 8-week-old GF mice were colonized with SPF-derived microbiota and were maintained under SPF housing conditions for three generations. Faecal samples were collected over time [8, 10, 12 and 18 weeks] and frozen at -20°C for downstream analysis.

2.10. Human samples for microbiota profiling

A total of 133 faecal samples from 29 CD patients with up to 5-year follow-up following haematopoietic stem cell transplantation [HSCT] were included in the analysis. Fresh faecal samples were collected either at the clinic or at home

by the patients using a stool collection kit within 24 h prior to the study visit. Patients were instructed to keep the samples stored in the home freezer until transported to the study site, as described previously.²³ Clinical assessments with measurement of the Crohn's disease activity index [CDAI] and biomarkers including C-reactive protein and faecal calprotectin were performed at baseline [before HSCT]. Metagenomic DNA extraction and 16S rRNA gene sequencing profiling were performed as described previously.²³

2.11. High-throughput 16S rRNA gene amplicon sequencing

Metagenomic DNA was extracted as previously described.²⁴ Briefly, cells were mechanically lysed in DNA stabilization buffer and extracted using phenol/chloroform/isoamyl alcohol [25:24:1, by vol.]. Following heat treatment of cells and centrifugation, supernatants were treated with RNase. DNA was purified with a NucleoSpin gDNA Clean-up Kit [Macherey-Nagel], following the manufacturer's instructions. Amplification with primers 341F-ovh and 785r-ovh and sequencing of the V3/V4 region of 16S rRNA genes was performed as previously described.^{25,26} In total, 227 porcine and 98 mouse samples were sequenced in paired-end mode [PE275] using a MiSeq system [Illumina] according to the manufacturer's instructions.

2.12. Amplicon sequence analysis

Raw 16S rRNA amplicon reads were pre-processed using the Integrated Microbial Next Generation Sequencing pipeline.²⁷ Five nucleotides on the 5' end and 3' end were trimmed for the R1 and R2 read [trim score 5] and an expected error rate of 1. Detected chimeric sequences were removed using UCHIME.²⁸ Sequences with relative abundance <0.25% and <300 and >600 nucleotides were excluded from analysis. A zero-radius operational taxonomic unit [zOTU] table was constructed considering all reads before quality filtering. Downstream analysis was performed using Rhea.²⁹ Taxonomy assignment was done using RDP classifier version 2.11 and confirmed using the SILVA database.³⁰ For phylogenetic analyses, maximum-likelihood trees were generated by FastTree based on MUSCLE alignments in MegaX.³¹ Alpha-diversity analysis was computed using community richness and Shannon's effective number of species. Beta-diversity analysis was performed using generalized UniFrac distances. Permutational multivariate analysis of variance [PERMANOVA] was performed for statistical evaluation of beta-diversity.

3. Results

3.1. Generation of *TNF^{ΔARE}* pigs

Binding motifs of RNA-degrading factors in the 3'-UTR of the *TNF* gene were identified by sequence alignments with human and murine orthologues. The tumour necrosis factor [TNF] class II AREs, which possess at least two overlapping UUAUUUA[U/A][U/A] nonamers,³² were located at position 445–516 bp downstream of the TNF stop codon. The CDEs were detected at positions 501–518 bp [CDE1] and 575–589 bp [CDE2] downstream of the stop codon.

Excision of the ARE and CDE1 sequences was performed by microinjection of a Cas9 expression vector, which also encodes the two gRNAs, into *in vitro* generated porcine zygotes [Figure 1A]. Five embryo transfers were carried out, resulting in two pregnancies and the birth of ten piglets of

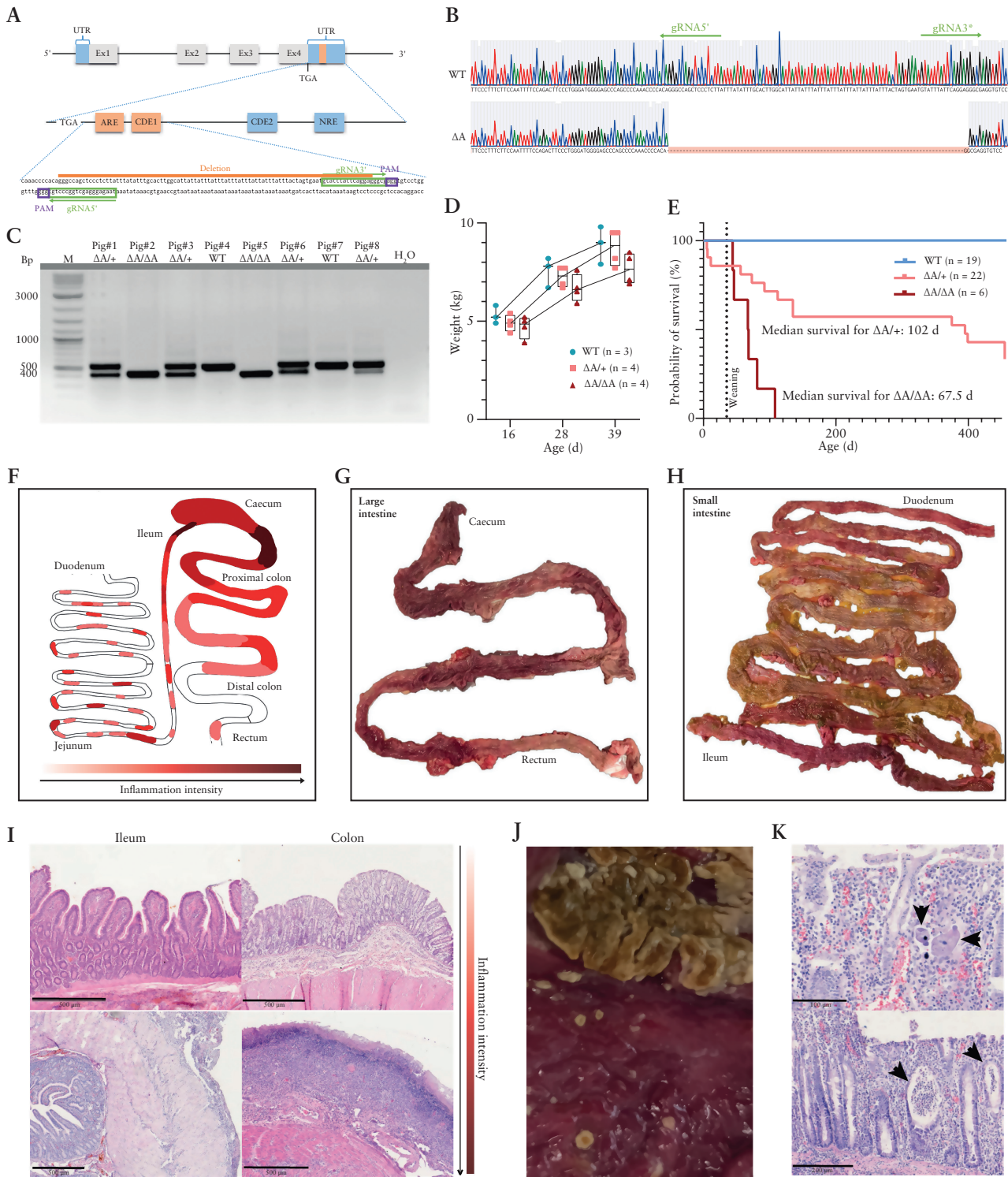


Figure 1. [A] Genome editing strategy for the deletion of the ARE and CDE1 elements. Expanded view shows the 3'-untranslated region [UTR] and excised sequence with the gRNA binding sites [marked in green]. ARE, CDE and NRE elements are shown as boxes, and the excised fragment [93 bp] is marked in orange. [B] Sanger sequencing showing expected excision of 93 bp. [C] Genotyping PCR of genome-edited founder piglets [pigs 1–8 from one of two litters born]. Expected size for the amplified wild-type TNF fragment of 524 bp, and for *TNF^{ΔARE}* of 431 bp. M, size marker. [D] Weight gain of wild-type, hetero- and homozygous *TNF^{ΔARE}* sibling pigs aged 16–39 days. [E] Kaplan–Meier curve indicating the time point at which animals were killed due to deteriorating health. The median survival times for euthanized *TNF^{ΔARE/+}* and *TNF^{ΔARE/ΔARE}* pigs are given. [F] Schematic representation of intestinal tract and sites of inflammation. Darker red colouring indicates sites of increased inflammation. [G, H] Representative images of inflamed large and small bowel. Macroscopic signs of inflammation were continuous throughout the large intestine, and segmental in the small intestine. [I] Representative images of H&E-stained colonic and ileal gut sections. Shown are mildly inflamed [top] and highly inflamed [bottom] tissue sections with crust formation [colon] and serositis [ileum]. Scale bars = 500 μm. [J] Diptheritic membranes in the caecum of a *TNF^{ΔARE/ΔARE}* pig. [K] Histopathological findings of invasive *Balantidium coli* [top] and crypt abscesses [bottom]. Scale bars = 100 μm [top] and 200 μm [bottom].

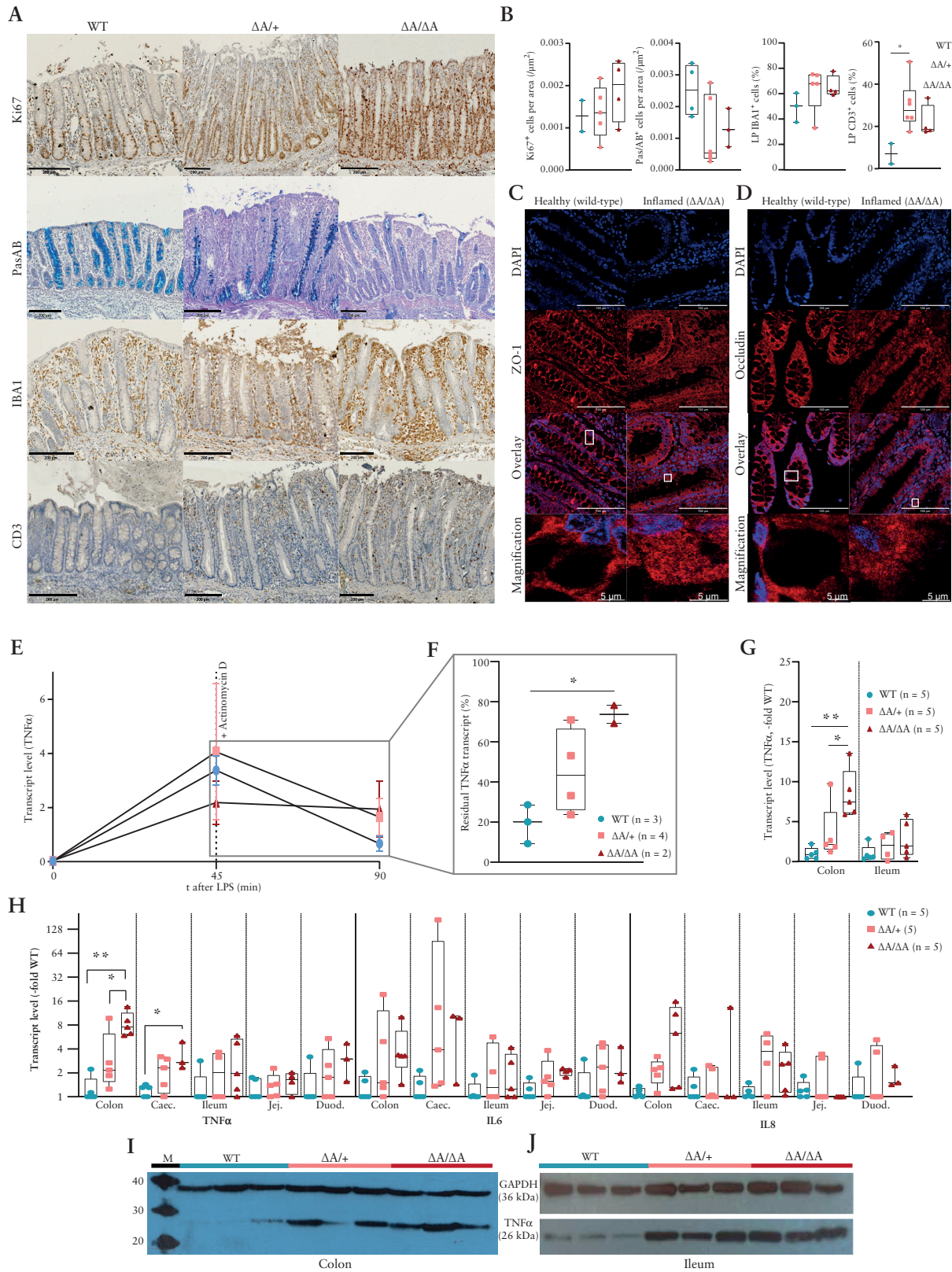


Figure 2. [A, B] Immunohistology and statistical evaluation of colon samples from wild-type and $TNF^{\Delta ARE}$ pigs showing an increase in Ki67⁺, CD3⁺ and IBA1⁺ cells and decrease in Pas/AB⁺ cells. Scale bars = 200 μm . [C, D] Confocal laser immunofluorescence scanning microscopy images of colonic sections stained for DAPI and ZO-1 or Occludin, respectively. Scale bars = 100 μm . Representative single cells were selected and shown magnified. Original signal intensities were adjusted for clear visualization of defined or diffuse antigen localization. [E, F] TNF mRNA levels and mRNA half-life assessed in macrophages from wild-type and $TNF^{\Delta ARE}$ pigs. [G] Comparison of TNF transcript levels in colonic and ileal mucosal biopsy samples shown as multiples of the average wild-type value. [H] Comparison of TNF , $IL6$ and $IL8$ mRNA levels in intestinal samples shown as multiples of the average wild-type value on a \log_2 scale. Caec, caecum; Duod, duodenum; Jej, jejunum. [I, J] TNF and GAPDH protein expression in colonic [K] and ileal samples [L] from three wild-type, three $TNF^{\Delta ARE/+}$ and three $TNF^{\Delta ARE/\Delta ARE}$ pigs. M, size marker.

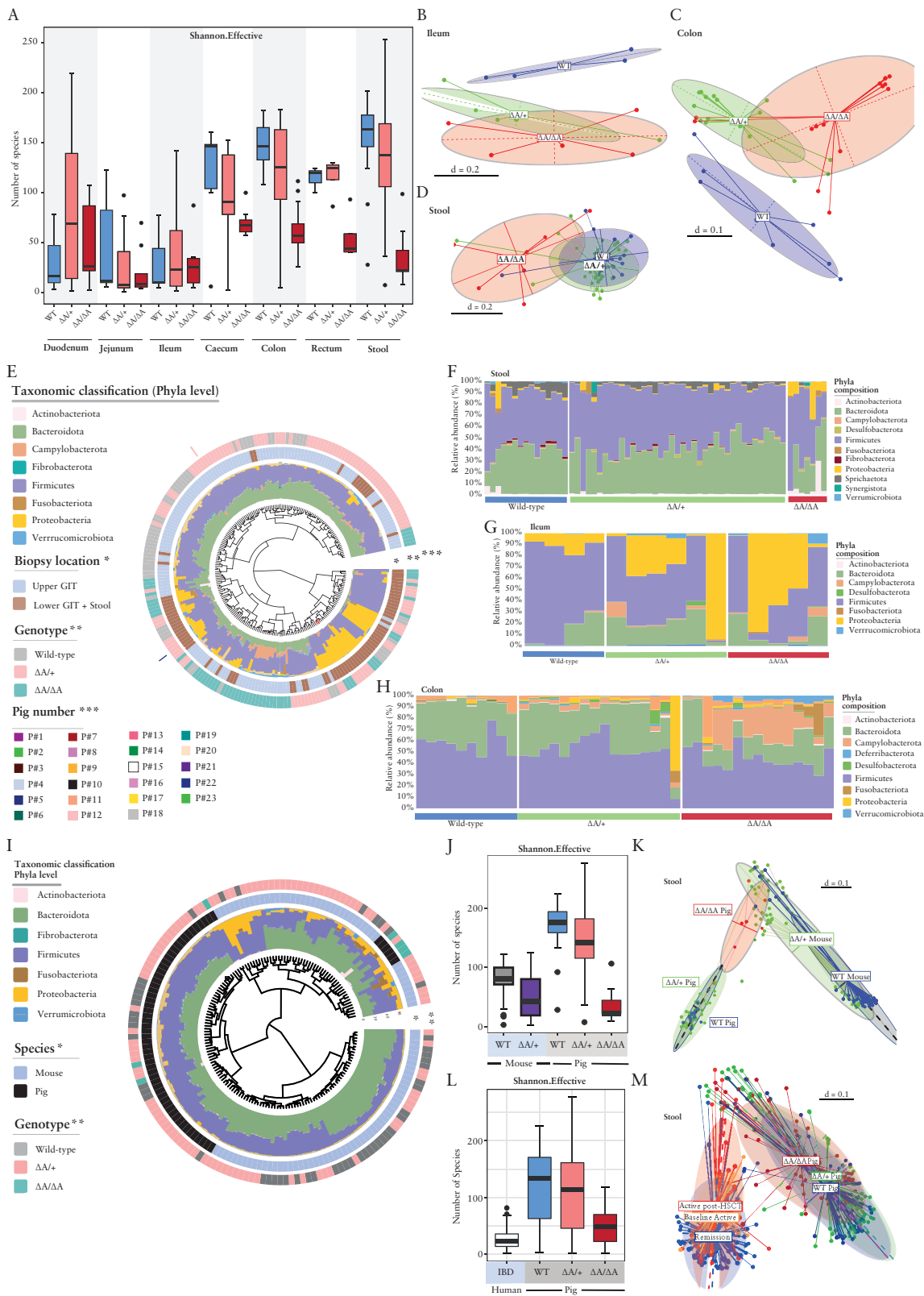


Figure 3. [A] Alpha-diversity of the luminal and mucosa-associated microbiota. Shannon an effective number of species. Sample locations and genotypes are indicated. [B–D] Multidimensional scaling [MDS] plots of microbial profiles of faecal, ileal and colonic samples stratified by genotype, respectively. [E] Phylogenetic tree showing the similarities between microbiota profiles based on generalized UniFrac distances in luminal [$n = 61$] and mucosa-associated microbiota [$n = 166$] derived from 23 pigs [seven wild-type, 16 $TNF^{\Delta ARE}$]. Individual taxonomic composition at the phylum level is shown as stacked bar plots around the phylogram. Innermost ring shows stratification based on sample type, upper GI tract samples [blue] and lower GI tract and stool samples [brown] and denoted by an asterisk [*]; the second ring shows stratification based on genotype, wild-type [grey], $TNF^{\Delta ARE/+}$ [pink] and $TNF^{\Delta ARE/\Delta ARE}$ [green] and denoted by two asterisks [**]. Bars in the outer ring of the figure indicate samples derived from each pig and denoted by three asterisks [***]. [F–H] Taxonomic composition at the phylum level in faecal, ileal and colonic samples stratified by genotype. [I] Phylogenetic tree

which two showed biallelic excision of the *ARE/CDE1* sequence [$TNF^{\Delta ARE/\Delta ARE}$, pigs 2 and 5], and five a monoallelic deletion [$TNF^{\Delta ARE/+}$, pigs 1, 3, 6, 8 and 9] [Figure 1B and C]. Two of the latter piglets [nos. 8, 9] showed in addition mosaicism and/or InDel mutations on the second allele, which was eliminated from the line after breeding with wild-type animals. The founder animals [nos. 6, 8, 9] used for breeding were screened for the five most likely off-targets and none were detected. Breeding resulted in 11 $TNF^{\Delta ARE/+}$ F1 and ten F2 offspring [seven $TNF^{\Delta ARE/+}$, three $TNF^{\Delta ARE/\Delta ARE}$]. A total of 13 male and ten female $TNF^{\Delta ARE/+}$, and two male and three female $TNF^{\Delta ARE/\Delta ARE}$ piglets were born. All progeny carried the identical sequence of the mutant allele.

3.2. $TNF^{\Delta ARE}$ pigs show clinical manifestations and inflammatory alterations of the intestine

After weaning, ~50% of $TNF^{\Delta ARE/+}$ animals showed reduced weight gain, and increased Bristol stool score that positively correlated with faecal calprotectin levels [Pearson's r : 0.5242; p_{adjusted} : 0.51]. This phenotype was more pronounced in $TNF^{\Delta ARE/\Delta ARE}$ pigs [Figure 1D; Supplementary Figure S1A and B]. Affected heterozygous and homozygous pigs were killed when termination criteria [chronic diarrhoea, severe weight loss, apathy] manifested. Median lifespan was 102 days for heterozygous $TNF^{\Delta ARE/+}$ pigs and 67.5 days for homozygous $TNF^{\Delta ARE/\Delta ARE}$ pigs [Figure 1E]. Macroscopically, $TNF^{\Delta ARE}$ animals had a more fragile intestinal wall when sampled and showed intestinal oedema and haemorrhage throughout the colon, segmental in the small intestine, frequently including the caecum [Figure 1F–H]. As with mice, inflammation intensity varied between pigs of the same genotype [Figure 1I]. In $TNF^{\Delta ARE/\Delta ARE}$ pigs the most severe alteration was ulcerative enteritis, sometimes covered with diphtheritic membranes in the caecum [Figure 1J]. Microscopically, 67% [4/6] of pathologically evaluated $TNF^{\Delta ARE/+}$ animals showed ileitis and/or colitis with mixed infiltrations of the lamina propria often extending into the tela submucosa accompanied by fibrinopurpurative serositis [Figure 1I]. In rare cases, extensive crypt abscesses [Figure 1K] and frequent herniation of crypts throughout the lamina muscularis mucosae or ulceration of the lamina propria mucosae with mixed infiltration and development of fibroangioblastic granulation tissue were observed. As expected from the macroscopic analysis, $TNF^{\Delta ARE/\Delta ARE}$ pigs showed a higher degree of intestinal abnormalities, including strong ulcerative inflammation with crust formation. In one case, an invasion of *Balantidium coli* into the mucosa was observed [Figure 1K].

Immunohistochemistry confirmed increased cell proliferation [Ki67⁺], increased leukocyte and lymphocyte infiltrations [IBA1⁺, CD3⁺], and decreased number of mucus-secreting goblet cells [Pas/AB⁺] in inflamed areas, especially in the ileocolonic region [Figure 2A and B]. Confocal laser immunofluorescence microscopy revealed a diffuse re-localization of tight junction proteins ZO-1 and occludin in inflamed tissue

[Figure 2C and D], and reduced protein levels for ZO-1 and occludin in the proximal colon of most $TNF^{\Delta ARE}$ mutants compared to wild-type pigs [Supplementary Figure S1B–D]. Complete blood counts revealed an increased monocyte count without significant changes in total white blood cells, basophilia, increased urea/creatinine ratio, hypoalbuminaemia and elevated serum Cu/Zn [Supplementary Figure S1F]. No signs of rheumatoid arthritis were observed.

3.3. Deletion of *ARE/CDE1* results in increased *TNF*-mRNA half-life, transcript abundance and protein levels

TNF is expressed by many different cell types, with highest expression in cells of the monocytic lineage, such as macrophages.³³ Therefore, macrophage cultures were established from PBMCs to investigate if the *TNF* mutation affects mRNA half-life. Transcription of *TNF* in macrophages was stimulated with LPS and inhibited after 45 min by the addition of actinomycin D. Prior to stimulation, *TNF* mRNA levels were slightly higher in macrophages isolated from $TNF^{\Delta ARE/\Delta ARE}$ and $TNF^{\Delta ARE/+}$ pigs compared to controls [2- and ~1.2-fold]. LPS stimulation resulted in an increase in *TNF* transcript levels at 45 min compared with resting macrophages in all genotypes. Inhibition of transcription through addition of actinomycin D resulted in a decrease of *TNF* mRNA levels. After 45 min of incubation with actinomycin D, the detected transcript levels were ~0.19% [wild-type], ~0.45% [$TNF^{\Delta ARE/+}$] and ~0.74% [$TNF^{\Delta ARE/\Delta ARE}$] compared to levels before the addition of this transcription inhibitor [Figure 2F and G]. Thus, the calculated half-lives of *TNF* mRNA in macrophages were ~19 min for wild-type, ~58 min for heterozygous and ~708 min for homozygous $TNF^{\Delta ARE}$ pig samples. Consistent with these results, colonic *TNF* mRNA expression was 7.4-fold higher [p_{adj} = 0.0027] in $TNF^{\Delta ARE/\Delta ARE}$ pigs and 2.2-fold [not significant] higher in $TNF^{\Delta ARE/+}$ swine compared to wild-type pigs [Figure 2H and I]. The elevated *TNF* mRNA expression resulted in increased *TNF* protein level in the colon and ileum of $TNF^{\Delta ARE}$ pigs, as shown by Western blot [Figure 2J and K].

Next, the effect of the increased *TNF* expression on its downstream targets was assessed. In colon tissue from $TNF^{\Delta ARE}$ pigs, mRNA expression of the key pro-inflammatory cytokine interleukin-6 [IL-6]³⁴ was 3.4-fold increased and the potent neutrophil chemoattractant IL-8³⁵ was 6.3-fold increased compared to wild-type controls. The increase in transcript abundance of all three target genes was observed throughout the gut, but most markedly in the ileocolonic region [Figure 2I].

3.4. Intestinal inflammation is linked to luminal and mucosa-associated bacterial dysbiosis in $TNF^{\Delta ARE}$ pigs

The relevance of dysbiotic microbial communities in initiating CD-like inflammation in $TNF^{\Delta ARE}$ mice was previously shown.³⁶ To characterize the changes in intestinal microbiota

showing the similarities between microbiota profiles based on generalized UniFrac distances in luminal microbiota derived from wild-type and $TNF^{\Delta ARE}$ pigs and mice. Individual taxonomic composition at the phylum level is shown as stacked bar plots around the phylogram. Innermost ring shows stratification based on species, mouse or pig; and the outer ring shows stratification based on genotype, wild-type [grey], $TNF^{\Delta ARE/+}$ [pink] and $TNF^{\Delta ARE/\Delta ARE}$ [green]. [J] Alpha-diversity of luminal microbiota from wild-type and $TNF^{\Delta ARE}$ pigs and mice is shown as Shannon effective number of species. [K] MDS plot of microbial profiles of faecal samples stratified by species [mouse or pig] and genotype, respectively. [L] Alpha-diversity of luminal and mucosal microbiota from human IBD patients and wild-type and $TNF^{\Delta ARE}$ pigs is shown as Shannon effective number of species. [M] MDS plot of microbial profiles of samples stratified by species [human or pig] and disease activity or genotype, respectively.

composition in relation to inflammation severity in $TNF^{\Delta ARE}$ pigs, we performed 16S rRNA gene sequencing on 166 mucosal tissue biopsies and 61 stool samples from seven wild-type, ten $TNF^{\Delta ARE/+}$ and six $TNF^{\Delta ARE/\Delta ARE}$ pigs. Samples were obtained from defined positions along the gastrointestinal tract. The microbial signatures were then compared with luminal and mucosal samples obtained from $TNF^{\Delta ARE/+}$ mice and a previously published cohort of human IBD patients.²³

Alpha-diversity was reduced in the large intestine and jejunum of $TNF^{\Delta ARE}$ pigs, while it was enriched in duodenum and ileum [Figure 3A]. Beta-diversity analysis showed separation of microbial profiles in ileal and colonic mucosa of wild-type, $TNF^{\Delta ARE/+}$ or $TNF^{\Delta ARE/\Delta ARE}$ pigs, which was weakly reflected in stool [Figure 3B–D]. Comparing individual microbiota compositions confirmed diverse ecosystems dominated by the two major phyla Firmicutes and Bacteroidetes in mucosal biopsies from duodenum, jejunum and ileum (upper gastrointestinal [GI] tract) in contrast to faecal microbiota or colon and cecum mucosal biopsies [lower GI tract] which were dominated by Firmicutes and Proteobacteria [Figure 3E, innermost ring and bar plots]. Microbiota profiling showed clear clustering in terms of inflammation severity in the different genotypes [Figure 3E, middle ring]. Longitudinal microbial profiling of luminal and mucosa-associated microbiota showed individual-specific clustering of microbiota composition [Figure 3E, outermost ring]. Taxonomic classification at the phylum level showed significantly increased relative abundance of the phylum Proteobacteria in faecal and ileal-associated bacterial communities of $TNF^{\Delta ARE}$ pigs compared to wild-type littermates [Figure 3F And G]. On the other hand, an enrichment of Fusobacteriota and Campylobacterota was observed in colon-associated microbial communities of $TNF^{\Delta ARE}$ pigs [Figure 3H]. Linear discriminant analysis effect size [LEfSe] analysis showed an enrichment in members of the genera *Helicobacter*, *Megasphaera*, *Campylobacter*, *Desulfovibrio*, *Alistipes* and *Lachnospirillum* among others in faecal or mucosa-associated bacteria of $TNF^{\Delta ARE}$ pigs compared to wild-type littermates [Supplementary Figure S2A–C].

Calprotectin protein concentrations were measured in faeces from highly and mildly inflamed pigs for two consecutive post-weaning time points t1 and t2 to examine whether changes in faecal bacterial composition precede inflammation. The stool samples were classified as severely ['High'] or mildly ['Low'] inflamed, based on the calprotectin concentration with a threshold of 30 ng/mL [Supplementary Figure S2D]. At t1, 2/7 [29%] and at t2, 4/7 [57%] specimens had a calprotectin concentration above 30 ng/mL in the stool samples [Figure S2D]. Overall, the average concentration of calprotectin was 1.6-fold [n.s.] higher at t2 compared to t1. β -Diversity analysis revealed weak inflammation-dependent shifts of microbiota profiles [Supplementary Figure S2E]. Calprotectin levels at t2 had a weak impact on the microbiota profiles of the respective samples at t1. Samples that were highly inflamed at t2 ['HI'] more closely clustered together with the respective samples at t1 when compared to samples that were mildly inflamed at t2 ['MI'], suggesting that a change in the gut microbiome precedes the inflammation detectable in the stool [Supplementary Figure S2F].

The comparison of luminal microbiota between $TNF^{\Delta ARE}$ pigs and mice showed clear separation of microbiota profiles with a subset of $TNF^{\Delta ARE/\Delta ARE}$ pigs clustering with $TNF^{\Delta ARE/+}$ mice, suggesting a species-independent microbial signature of intestinal inflammation. As expected, wild-type pigs showed significantly

higher bacterial community richness and diversity compared to mice, while $TNF^{\Delta ARE/\Delta ARE}$ pigs showed the lowest number of species [Figure 3I–K]. LEfSe analysis identified a set of bacterial genera that are significantly differential between $TNF^{\Delta ARE/+}$ pigs and mice. While in mice an increased abundance of *Alistipes*, *Bacteriodes*, *Escherichia coli*, *Fusobacterium* was observed, the $TNF^{\Delta ARE/+}$ pigs showed more *Prevotella*, *Lactobacillus*, *Treponema* and *Megasphaera*, among others [Supplementary Figure S2G]. Similar results were observed when comparing $TNF^{\Delta ARE}$ pigs and the human IBD cohort. We found clear species-specific clustering of microbiota profiles [Supplementary Figure S2H] and a higher bacterial diversity in porcine samples [Figure 3L]. Notably, samples derived from IBD patients with active disease clustered with a subset of $TNF^{\Delta ARE/\Delta ARE}$ and $TNF^{\Delta ARE/+}$ pigs [Figure 3M], supporting the assumption of a species-independent microbial signature of IBD.

4. Discussion

Despite decades of basic and clinical research, IBD remains a global health problem with rising incidence and prevalence.² The mouse models for CD-like chronic inflammation are ideally suited to basic research, to elucidate the molecular basis of the disease and to assess the interplay between gut epithelium, inflammation and the microbiome. This has undoubtedly contributed to considerable improvements in the treatment of CD.^{22,36} However, major differences between humans and rodents especially with regard to nutrient requirements, the physiology of the GI tract, as well as immunological and metabolic differences hamper the translation of findings into the clinic.^{7,37–40} There is a need for more physiologically relevant translational models. Both humans and pigs are omnivorous and share similarities related to anatomical features of the GI tract. Pigs are a widely accepted model for nutrition research, intestinal microbiota and gut barrier function.¹¹ All of this makes them an ideal model for IBD.

$TNF^{\Delta ARE}$ pigs show symptoms characteristic of IBD, including chronic diarrhoea and weight loss, aberrant intestinal morphology and changes in intestinal epithelial cell composition.¹ Similar to human CD patients, transmural skip lesions within the intestinal tract with ileocolitic predominance, reduced numbers of PAS/AB⁺ cells, increased cell proliferation and increased immune cell infiltrations in inflamed areas were observed.¹ The blood tests were indicative of intestinal inflammation, malnutrition, gastrointestinal haemorrhage and active disease.^{41–43} Together with the observed diffuse patterning and lower concentration of tight junction proteins in most $TNF^{\Delta ARE}$ pigs, fibrinous exudates and gut-penetrating *Balantidium coli*, our findings suggest a disruption of the intestinal barrier with loss of mucosal tolerance. A disrupted intestinal barrier not only facilitates microbial invasion into intestinal tissues but also allows increased passage of oxygen into the intestinal lumen with devastating effects on the intestinal microbiota.^{44,45} In line with these data, we observed a reduction in the often obligate anaerobic genera of Bacteroidota and Firmicutes and an increase in the largely facultatively anaerobic Proteobacteria with a concomitant decrease in bacterial diversity in the ileum of $TNF^{\Delta ARE}$ pigs, findings previously reported for IBD patients.^{44,46} Furthermore, an increase of Campylobacterota along with a decline of Bacteroidota in the colon was previously associated with an increased risk of IBD.^{47,48} Compositional changes in the stool microbiota were found to be weakly influenced by future

calprotectin levels, indicating that changes in the faecal microbiota composition precede the onset of inflammation. This is consistent with previous findings in IBD patients, where the difference in mucosal samples was even more pronounced.⁴⁹

The early disease onset shortly after weaning appears to contrast with humans, in which the majority of early-onset IBD patients have an age of ~10 years at diagnosis.⁵⁰ The ‘weaning reaction’ of the immune system in response to concomitant microbiota alterations is accompanied by an upregulation of TNF, which is thought to be a disease trigger in the *TNF^{ΔARE}* animal and probably contributes to the early disease onset in the swine model.⁵¹ As in mice the reasons why only about 50% of heterozygous porcine mutants show disease manifestations remain to be elucidated. In the mouse model, it has been reported that the abundance of an immunomodulatory commensal correlates with ileitis disease severity, although a cross-model and cross-species significance remains controversial.⁵²

Regarding the TNF mRNA decay kinetics, the pig model shows some differences to the IBD mouse published by Kontoyiannis *et al.*,⁵³ in which only the ARE has been deleted while in the swine model the ARE and CDE1 sequence was removed. We observed a comparable effect of LPS stimulus on the transcription of TNF in PBMC-derived macrophages, but a more pronounced increase in transcript half-life. This is in line with a recently published mouse model showing that disease severity increased with concurrent deletions of ARE and CDEs, where the authors suggested an impact of the mutations on post-transcriptional TNF mRNA regulation.⁵⁴

Importantly, the *TNF^{ΔARE}* pigs show transmural inflammation not only in the terminal ileum as in *TNF^{ΔARE}* mice, but also a robust disease manifestation in the proximal colon as seen in humans. This is probably due to the fact that pigs, like humans, have their primary site for ingesta fermentation in the colon compared to caecal fermentation in mice. Since luminal microbes mediate intestinal fermentation, its anatomical localization directly affects the constituents of the gut microbiota and thus microbe–host interactions.⁵⁵ Host-specific colonization of bacterial communities was also confirmed by the separation between microbiota profiles in the two models. On the other hand, clustering of the luminal and mucosal microbiota from *TNF^{ΔARE/+}* mice or a subset of human IBD patients with active disease and *TNF^{ΔARE/ΔARE}* pigs with strong inflammation suggests a species-independent composition of the microbiota correlating with inflammation severity.

In mice and humans, microbial composition is typically measured from faecal samples. It does not necessarily reflect bacterial diversity along the GI tract. In line with this, the cross-genotype comparison of bacterial microbiota alterations in stool provided only a weak reflection of the conditions observed for affected intestinal mucosal biopsies. The option to carry out repeated endoscopies or work with cannulated pigs will provide a better understanding of the local interactions between gut microbiota, inflammation, and nutritional or therapeutic interventions. None of this is possible in human patients. Like mice, pigs can be reared under GF conditions. Importantly, microbiome transfer from humans to pigs results in a gut microbiota closely resembling that of the human donor.¹⁴ Novel diagnostic technologies can be assessed at the human scale.⁹

In summary, this work reports on *TNF^{ΔARE}* pigs as a translational animal model for IBD. The *TNF^{ΔARE}* pigs recapitulate major characteristics of human CD, including ulcerative transmural ileocolitis, increased abundance of proinflammatory cytokines, impaired integrity of the intestinal epithelial cell

barrier, immune cell infiltration and changes in dysbiotic microbial communities. This model enables human-scale and long-term studies to assess diagnostic, nutritional or microbial interventions. The pig model is not intended to substitute the mouse models, but rather to fill the gap for translating findings to the clinic. The value of pig models for digestive disease research has been frequently demonstrated,^{9,56,57} and the *TNF^{ΔARE}* pigs will undoubtedly become an important asset for patient-relevant translational CD studies.

Funding

The study was funded by the Deutsche Forschungsgemeinschaft [DFG, German Research Foundation] – Projektnummer 395357507—SFB 1371.

Conflict of Interest

The authors declare no conflicts of interest.

Acknowledgments

The authors would like to thank Lea Radomsky, Sara Robin, Monika Heilmeyer and Benjamin Strickland for their technical support and Viola and Steffen Löbnitz for animal husbandry. We would also like to acknowledge the Center for Advanced Light Microscopy [CALM, Technical University of Munich, Germany] for providing confocal laser scanning microscopes.

Author Contributions

T.W., K.Fli., D.H. and A.S. designed research; T.W., B.Kli., W.L., A.G., T.F. and A.M. performed research; T.W., A.M., K.Fli., K.S., K. Fis. and A.S. analysed data; T.W., K. Fli, T. Fli, K. Fis., K.S., A.M, K.S, D.H. and A.S. wrote the paper.

Data Availability

The accession number for the IBD patient cohort [HSCT-treated Crohn’s disease patients] raw 16S rRNA gene sequencing data reported in this paper was accessed via the Sequence Read Archive [SRA: PRJNA565903]. The accession number for the raw 16S rRNA gene sequencing data as well as metadata information of the pig and mouse models reported in this paper are available via the Sequence Read Archive [SRA: PRJNA907809]. Software programs used to analyse the data are either freely or commercially available. All other data relevant to the study are included in the article. Additional data are available on request.

Supplementary Data

Supplementary data are available online at *ECCO-JCC* online.

References

1. Chang JT. Pathophysiology of inflammatory bowel diseases. *N Engl J Med* 2020;383:2652–64.
2. Ng SC, Shi HY, Hamidi N, *et al.* Worldwide incidence and prevalence of inflammatory bowel disease in the 21st century: a systematic review of population-based studies. *The Lancet* 2017;390:2769–78.

3. Jostins L, Ripke S, Weersma RK, *et al*; International IBD Genetics Consortium (IBDGC). Host-microbe interactions have shaped the genetic architecture of inflammatory bowel disease. *Nature* 2012;491:119–24.
4. Neurath MF. Animal models of inflammatory bowel diseases: illuminating the pathogenesis of colitis, ileitis and cancer. *Dig Dis* 2012;30:91–4.
5. Jergens AE, Sonea IM, O'Connor AM, *et al*. Intestinal cytokine mRNA expression in canine inflammatory bowel disease: a meta-analysis with critical appraisal. *Comp Med* 2009;59:153–62.
6. Gozalo A, Dagle GE, Montoya E, Weller RE. Spontaneous terminal ileitis resembling Crohn disease in captive tamarins. *J Med Primatol* 2002;31:142–6.
7. Taylor NP. *Synlogic scraps ammonia-lowering drug after early phase fail*, 2019. <https://www.fiercebiotech.com/biotech/synlogic-scraps-ammonia-lowering-drug-after-early-phase-fail>. Accessed March 7, 2022.
8. Flisikowska T, Merkl C, Landmann M, *et al*. A porcine model of familial adenomatous polyposis. *Gastroenterology* 2012;143:1173–1175.e7.
9. Rogalla S, Flisikowski K, Gorpas D, *et al*. Biodegradable fluorescent nanoparticles for endoscopic detection of colorectal carcinogenesis. *Adv Funct Mater* 2019;29:1904992.
10. Ziegler A, Gonzalez L, Blikslager A. Large animal models: the key to translational discovery in digestive disease research. *Cell Mol Gastroenterol Hepatol* 2016;2:716–24.
11. Roura E, Koopmans S-J, Lallès J-P, *et al*. Critical review evaluating the pig as a model for human nutritional physiology. *Nutr Res Rev* 2016;29:60–90.
12. Wylensek D, Hitch TCA, Riedel T, *et al*. A collection of bacterial isolates from the pig intestine reveals functional and taxonomic diversity. *Nat Commun* 2020;11:6389.
13. Forster SC, Kumar N, Anonye BO, *et al*. A human gut bacterial genome and culture collection for improved metagenomic analyses. *Nat Biotechnol* 2019;37:186–92.
14. Pang X, Hua X, Yang Q, *et al*. Inter-species transplantation of gut microbiota from human to pigs. *ISME J* 2007;1:156–62.
15. Xiao L, Estellé J, Kiilerich P, *et al*. A reference gene catalogue of the pig gut microbiome. *Nat Microbiol* 2016;1:16161.
16. Yang H, Wu J, Huang X, *et al*. ABO genotype alters the gut microbiota by regulating GalNAc levels in pigs. *Nature* 2022;606:358–367.
17. Concordet J-P, Haeussler M. CRISPOR: intuitive guide selection for CRISPR/Cas9 genome editing experiments and screens. *Nucleic Acids Res* 2018;46:W242–5.
18. Petersen B, Frenzel A, Lucas-Hahn A, *et al*. Efficient production of biallelic GGTA1 knockout pigs by cytoplasmic microinjection of CRISPR/Cas9 into zygotes. *Xenotransplantation* 2016;23:338–46.
19. Kurome M, Kessler B, Wuensch A, Nagashima H, Wolf E. Nuclear transfer and transgenesis in the pig. *Methods Mol Biol* 2015;1222:37–59.
20. Andersen CL, Jensen JL, Ørntoft TF. Normalization of real-time quantitative reverse transcription-PCR data: a model-based variance estimation approach to identify genes suited for normalization, applied to bladder and colon cancer data sets. *Cancer Res* 2004;64:5245–50.
21. Pfaffl MW, Tichopad A, Prgomet C, Neuvians TP. Determination of stable housekeeping genes, differentially regulated target genes and sample integrity: BestKeeper-Excel-based tool using pair-wise correlations. *Biotechnol Lett* 2004;26:509–15.
22. Khaloian S, Rath E, Hammoudi N, *et al*. Mitochondrial impairment drives intestinal stem cell transition into dysfunctional Paneth cells predicting Crohn's disease recurrence. *Gut* 2020;69:1939–51.
23. Merwaly A, Dunkel A, Waldschmitt N, *et al*. Integrated microbiota and metabolite profiles link Crohn's disease to sulfur metabolism. *Nat Commun* 2020;11:4322.
24. Bazanella M, Maier TV, Clavel T, *et al*. Randomized controlled trial on the impact of early-life intervention with bifidobacteria on the healthy infant fecal microbiota and metabolome. *Am J Clin Nutr* 2017;106:1274–86.
25. Kozich JJ, Westcott SL, Baxter NT, Highlander SK, Schloss PD. Development of a dual-index sequencing strategy and curation pipeline for analyzing amplicon sequence data on the MiSeq Illumina sequencing platform. *Appl Environ Microbiol* 2013;79:5112–20.
26. Lagkouvardos I, Kläring K, Heinzmann SS, *et al*. Gut metabolites and bacterial community networks during a pilot intervention study with flaxseeds in healthy adult men. *Mol Nutr Food Res* 2015;59:1614–28.
27. Lagkouvardos I, Joseph D, Kapfhammer M, *et al*. IMNGS: A comprehensive open resource of processed 16S rRNA microbial profiles for ecology and diversity studies. *Sci Rep* 2016;6:33721.
28. Edgar RC, Haas BJ, Clemente JC, Quince C, Knight R. UCHIME improves sensitivity and speed of chimera detection. *Bioinformatics* 2011;27:2194–200.
29. Lagkouvardos I, Fischer S, Kumar N, Clavel TR. A transparent and modular R pipeline for microbial profiling based on 16S rRNA gene amplicons. *PeerJ* 2017;5:e2836.
30. Quast C, Pruesse E, Yilmaz P, *et al*. The SILVA ribosomal RNA gene database project: improved data processing and web-based tools. *Nucleic Acids Res* 2013;41:D590–6.
31. Kumar S, Stecher G, Li M, Knyaz C, Tamura K. MEGA X: molecular evolutionary genetics analysis across computing platforms. *Mol Biol Evol* 2018;35:1547–9.
32. Barreau C, Paillard L, Osborne HB. AU-rich elements and associated factors: are there unifying principles? *Nucleic Acids Res* 2005;33:7138–50.
33. Parameswaran N, Patial S. Tumor necrosis factor- α signaling in macrophages. *Crit Rev Eukaryot Gene Expr* 2010;20:87–103.
34. Danese S, Vermeire S, Hellstern P, *et al*. Randomised trial and open-label extension study of an anti-interleukin-6 antibody in Crohn's disease (ANDANTE I and II). *Gut* 2019;68:40–8.
35. Grimm MC, Elsbury SK, Pavli P, Doe WF. Interleukin 8: cells of origin in inflammatory bowel disease. *Gut* 1996;38:90–8.
36. Schaubeck M, Clavel T, Calasan J, *et al*. Dysbiotic gut microbiota causes transmissible Crohn's disease-like ileitis independent of failure in antimicrobial defence. *Gut* 2016;65:225–37.
37. Kurtz CB, Millet YA, Puurunen MK, *et al*. An engineered *E. coli* Nissle improves hyperammonemia and survival in mice and shows dose-dependent exposure in healthy humans. *Sci Transl Med* 2019;11.
38. Moser A, Luongo C, Gould K, McNeley M, Shoemaker A, Dove WA. A mouse model for intestinal and mammary tumorigenesis. *Eur J Cancer* 1995;31:1061–4.
39. Lehr HA, Menger MD, Granger DN. Ischemia-reperfusion injury: enthusiasm in laboratory research but dilemma in clinical trials? *Circulation* 1994;90:1580.
40. Rogers CS, Hao Y, Rokhlina T, *et al*. Production of CFTR-null and CFTR-DeltaF508 heterozygous pigs by adeno-associated virus-mediated gene targeting and somatic cell nuclear transfer. *J Clin Invest* 2008;118:1571–7.
41. Guo C-H, Chen P-C, Yeh M-S, Hsiung D-Y, Wang C-L. Cu/Zn ratios are associated with nutritional status, oxidative stress, inflammation, and immune abnormalities in patients on peritoneal dialysis. *Clin Biochem* 2011;44:275–80.
42. Cherfane CE, Gessel L, Cirillo D, Zimmerman MB, Polyak S. Monocytosis and a low lymphocyte to monocyte ratio are effective biomarkers of ulcerative colitis disease activity. *Inflamm Bowel Dis* 2015;21:1769–75.
43. Felber S, Rosenthal P, Henton D. The BUN/creatinine ratio in localizing gastrointestinal bleeding in pediatric patients. *J Pediatr Gastroenterol Nutr* 1988;7:685–7.
44. Lloyd-Price J, Arze C, Ananthakrishnan AN, *et al*; IBDMDB Investigators. Multi-omics of the gut microbial ecosystem in inflammatory bowel diseases. *Nature* 2019;569:655–62.
45. Albenberg L, Esipova TV, Judge CP, *et al*. Correlation between intraluminal oxygen gradient and radial partitioning of intestinal microbiota. *Gastroenterology* 2014;147:1055–63.e8.
46. Rigottier-Gois L. Dysbiosis in inflammatory bowel diseases: the oxygen hypothesis. *ISME J* 2013;7:1256–61.

47. Hutchinson E. Risk of IBD increases after *Salmonella* or *Campylobacter* gastroenteritis. *Nat Rev Gastroenterol Hepatol* 2009;6:561561.–561.
48. Shao J, Li Z, Gao Y, et al. Construction of a ‘bacteria-metabolites’ co-expression network to clarify the anti-ulcerative colitis effect of flavonoids of *Sophora flavescens* Aiton by regulating the ‘host-microbe’ interaction. *Front Pharmacol* 2021;12:710052.
49. Glymenaki M, Singh G, Brass A, et al. Compositional changes in the gut mucus microbiota precede the onset of colitis-induced inflammation. *Inflamm Bowel Dis* 2017;23:912–22.
50. Benchimol EI, Mack DR, Nguyen GC, Snapper SB, Li W, Mojaverian N, Quach P, Muike AM. Incidence, outcomes, and health services burden of very early onset inflammatory bowel disease. *Gastroenterology* 2014;147:803–813.e7; quiz e14.e7; quiz e14-5.
51. Guo F, Cai D, Li Y, et al. How early-life gut microbiota alteration sets trajectories for health and inflammatory bowel disease? *Front Nutr* 2021;8:690073.
52. Metwally A, Jovic J, Waldschmitt N, et al. Diet prevents the expansion of segmented filamentous bacteria and ileo-colonic inflammation in a model of Crohn’s disease. *bioRxiv* 2022:2022.07.06.498810. doi:10.1101/2022.07.06.498810.
53. Kontoyiannis D, Pasparakis M, Pizarro TT, Cominelli F, Kollias G. Impaired On/off regulation of TNF biosynthesis in mice lacking TNF AU-rich elements. *Immunity* 1999;10:387–98.
54. Clayer E, Dalseno D, Kueh A, et al. Severe impairment of TNF post-transcriptional regulation leads to embryonic death. *iScience* 2020;23:101726101726.
55. Rose EC, Blikslager AT, Ziegler AL. Porcine models of the intestinal microbiota: the translational key to understanding how gut commensals contribute to gastrointestinal disease. *Front Vet Sci* 2022;9:834598.
56. Troya J, Krenzer A, Flisikowski K, et al. New concept for colonoscopy including side optics and artificial intelligence. *Gastrointest Endosc* 2022;95:794–8.
57. Yim JJ, Harmsen S, Flisikowski K, et al. A protease-activated, near-infrared fluorescent probe for early endoscopic detection of premalignant gastrointestinal lesions. *Proc Natl Acad Sci U S A* 2021;118.